NASA Technical Memorandum 102251

Computation of the Unsteady Facilitated Transport of Oxygen in Hemoglobin

Sanford Davis

January 1990

NASA

National Aeronautics and
Space Administration

Ames Research Center
Moffett Field, California 94035

Computation of the Unsteady Facilitated Transport of Oxygen in Hemoglobin

Sanford Davis, Ames Research Center, Moffett Field, California

January 1990

TABLE OF CONTENTS

SUMMARY

The transport of a reacting permeant diffusing through a thin membrane is extended to more realistic dissociation models. A new nonlinear analysis of the reaction-diffusion equations, using implicit finite-difference methods and direct block solvers, is used to study the limits of linearized and equilibrium theories. Computed curves of molecular oxygen permeating through hemoglobin solution are used to illustrate higher-order reaction models, the effect of concentration boundary layers at the membrane interfaces, and the transient buildup of oxygen flux.

INTRODUCTION

Membranes have been found to be very useful for separating both gaseous and aqueous mixtures. Artificial membranes with very selective separation properties are now commercially available and may find many applications in advanced life support systems for future space missions. The concentration and separation of aqueous wastes have been studied extensively using the reverse-osmosis process, which depends on the passive action of membrane systems (Lonsdale, 1986). Another, and very intriguing, aspect of membrane separation is the facilitated transport mechanism (Schultz, 1986). This mode of diffusive transport was discovered in experimental studies of oxygen diffusion through films of hemoglobin solution, and has been the subject of many studies. Facilitated transport depends on the action of a reversible chemical reaction to increase the flux of a permeant many times over that existing in a passive medium. This is a particularly effective method for the selective transport of specific molecules such as oxygen through a liquid membrane of hemoglobin in blood plasma. This paper presents a new analysis of facilitated transport in a particular biological process—the enhanced diffusion of oxygen using oxygenated hemoglobin as a carrier. This analysis should also be useful in the development of new carrier species, both natural and synthetic, for the efficient separation and concentration of gaseous components of life support systems (such as carbon dioxide) for long-duration space missions.

Hemmingsen and Scholander (1960) and Scholander (1960) demonstrated that the oxygen flux through thin liquid films is greatly enhanced by the presence of the protein hemoglobin. Furthermore, the degree of enhancement was shown to be sensitive to the oxygen concentration difference across the membrane. In an attempt to explain these important observations, many mathematical models were developed (Collins, 1960; Wang, 1961; Fatt and La Force, 1965; Friedlander, 1965). These early papers made the critical assumption that oxygen and hemoglobin were in chemical equilibrium across the film. This is a reasonable assumption for the oxygen-hemoglobin system for films thicker than about 100 microns. In the equilibrium state, the degree of facilitation can be simply computed with algebraic techniques or even estimated qualitatively using the oxygen dissociation curve.

The steady-state diffusion of oxygen through hemoglobin solution was computed for the case of nonequilibrium chemical reactions by Kutchai et al. (1970). The equations governing the process are a system of coupled nonlinear ordinary differential equations. Using a numerical algorithm based on the quasi-linearization scheme, they were able to predict the overall facilitation as well as the detailed distribution of oxygen and hemoglobin across the liquid membrane. The system of equations displays a boundary layer effect at the air/film interfaces which has been the source of past difficulties in the

analysis of these systems. In Kutchai et al. (1970), a special iteration scheme was developed to obtain converged solutions for increasing film thicknesses. An important conclusion of this work was that in vitro studies of facilitated transport are adequately predicted by equilibrium theories, but for systems of the dimensions of human erythrocytes, the more complex nonequilibrium analysis must be used since the effective film thickness cannot be accommodated by equilibrium theory.

Following these studies, a number of new analysis methods were introduced. A numerical scheme based on the concept of "local linearization" was introduced by Gonzalez-Fernandez and Atta (1981, 1982). An approach based on the finite element technique was used by Jain and Schultz (1982). This latter work, in particular, includes a very comprehensive discussion of the boundary-layer effect and introduces one particular method to treat this difficulty. On the analytical side, this problem has been treated as an example of a "singular perturbation" (Goddard et al., 1970; Schultz et al., 1974) where the governing differential equations are such that the highest derivative is multiplied by a small parameter. In the limiting case of an infinitely thick membrane, this parameter vanishes and the system is in chemical equilibrium. In this limit, it is not possible to satisfy all the boundary conditions, and this has been the source of some confusion in the past. This boundary-layer effect is also the basis for the term "stiffness" that has been used for this class of transport processes and it causes many difficulties in the solution of facilitated transport problems. (It is interesting that this is a relatively benign singular perturbation since the derivative of the unknown function is given as a boundary condition. Its limiting value, however, can easily be computed from equilibrium theory. In the original singular perturbation problem concerning the flow of a viscous fluid, the value of the function is given and its derivative is unknown. The limiting case is the nonphysical slip-flow solution with the derivative undefined.) All of the work mentioned above treats the steady-state transport and assumes that the chemical reaction is a second-order process.

The flow of oxygen across a thin film is not an instantaneous process and, in fact, the development time is a strong function of the system parameters. The study of unsteady facilitated transport is not as well developed as the steady problem. Recent studies of unsteady facilitated transport by Ruckenstein (1982) and Varanasi (1983) also used the local linearization method mentioned above and assumed second-order chemical reactions.

In this paper, the unsteady transport of oxygen across a hemoglobin solution with higher-order chemical reactions is studied using a finite-difference algorithm based on the method of time linearization. Before applying the algorithm, the governing systems of equations are recast into a first-order matrix-differential equation. This has the distinct advantage that all fluxes are treated as dependent variables and are computed directly as the solution evolves. Another advantage is that the transport of multiple permeant-species can be easily accommodated—the only change being the order of the matrices involved. A third advantage of the matrix approach is that the eigenvalue spectrum can be easily computed, which gives a good physical understanding of difficulties found in previous solution methods. It is shown that this problem is yet another example of a class of "stiff" problems that arise frequently in practical situations. The facilitated transport problem is stiff in the spatial sense, which means that eigenmodes of disparate scales are generated.

It has been demonstrated in the theory of nonequilibrium high-speed gas dynamics (Lomax and Bailey, 1967) that implicit numerical methods are almost mandatory when solving stiff problems. In this paper, an implicit algorithm based on a noniterative block-triadiagonal solver is implemented in the

2

development of an efficient solution process. A linearized form of the reaction-diffusion equation is derived that highlights the disparate time scales. This linearized system is used to develop an explicit formula for the size of the boundary layer region. In the following sections, solutions to the full nonlinear systems are presented for the oxygen-hemoglobin system and comparisons made with previously published results. The effect of initial conditions and physically plausible oxygen dissociation curves on the final steady-state flux is computed using the system parameters of Scholander (1960), Hemmingsen and Scholander (1960), and Kutchai et al. (1970).

THE OXYGEN DISSOCIATION CURVE AND FACILITATED TRANSPORT

A very important measure of the oxygen affinity of hemoglobin is its characteristic dissociation curve. In most theoretical treatments, a second-order reaction is assumed which restricts the curve to one branch of a hyperbola. This is a good approximation for oxygen transport through myoglobin, but is not as accurate for the cooperative binding that occurs in hemoglobin molecules. A simple analytical approximation to the oxygen dissociation curve is (Stryer, 1981, p. 67):

$$Y = \frac{\alpha^n pO_2^n}{\alpha^n pO_{2,0.5}^n + \alpha^n pO_2^n} \tag{1}$$

where Y is the ratio of oxyhemoglobin to the total hemoglobin present and α is the solubility coefficient (assuming Henry's Law). pO_2 is the partial pressure of oxygen (αpO_2 is its concentration in moles/cc) and $pO_{2,0.5}$ is the oxygen partial pressure when $Y = 0.5$, which is a commonly used reference point for the dissociation curve. The effect of the exponent n will be investigated for the cases $n = 1$ (hyperbolic dissociation curve) and $n = 2.8$ (Hill's exponent, sigmoidal dissociation curve).

Dissociation curves are shown in figure 1 for (1) an approximate second-order curve that matches the 50% saturation point in Scholander (1960), (2) an approximate 3.8th-order reaction that matches the same 50% saturation point, and (3) an approximate 3.8th-order reaction that matches the 3.8th-order reaction for hemoglobin at physiological conditions. The experimental data show a very rapid rise to 100% saturation that is better matched to the sigmoidal shaped curve than the hyperbola. The increased oxygen affinity for the in vitro experiments referenced in Scholander (1960) may be due to the absence of certain substances in the intact erythrocytes.

These curves can also be used to assess the relative degree of facilitation assuming equilibrium conditions throughout the film. The slope of a line from the origin to any point on the dissociation curve is proportional to the facilitation factor for the transport of oxygen from the indicated value of pO_2 to a vacuum. It is clear from figure 1 that for $pO_2 < pO_{2,0.5}$ the facilitation factor for a second-order reaction is increased relative to that using Hill's exponent, while the reverse is true for $pO_2 > pO_{2,0.5}$. Similar comparisons can be made for other oxygen concentration differences. Further details of the facilitation process for nonequilibrium conditions must be made with the aid of the governing differential equations.

GOVERNING EQUATIONS AND LINEARIZED FORMULATION

The continuity equation for the transient diffusion of a dilute permeant (oxygen) in a solvent that supports a reversible chemical reaction (hemoglobin solution) is generally expressed as a reaction-diffusion equation:

$$\frac{\partial C}{\partial t} = D\nabla^2 C - R \qquad (2)$$

where C is the species concentration, D is the diffusivity, and R is the rate of reaction of the species C. In the case of a one-reaction/three-species system in a one-dimensional membrane, equation 2 is replaced by three coupled partial differential equations:

$$\frac{\partial [O_2]}{\partial t} = \frac{D_A}{L^2} \frac{\partial^2 [O_2]}{\partial x^2} - R$$

$$\frac{\partial [Hb]}{\partial t} = \frac{D_B}{L^2} \frac{\partial^2 [Hb]}{\partial x^2} - R \qquad (3)$$

$$\frac{\partial [HbO_2]}{\partial t} = \frac{D_B}{L^2} \frac{\partial^2 [HbO_2]}{\partial x^2} + R$$

The bracketed quantities denote concentrations of oxygen, hemoglobin, and oxygenated hemoglobin, respectively. The diffusivity for hemoglobin and oxygenated hemoglobin are assumed equal. The main justification for this assumption is the much greater molecular weight of the hemoglobin protein compared with the oxygen molecule (Kutchai et al., 1970). The distance x across the membrane is normalized by the thickness L. The solution to equation 3 must satisfy the following boundary conditions at every instant of time:

$$[O_2] = C_0 \quad \frac{\partial [HbO_2]}{\partial x} = \frac{\partial [Hb]}{\partial x} = 0 \quad @ \; x = -0.5$$

$$(3a)$$

$$[O_2] = C_1 \quad \frac{\partial [HbO_2]}{\partial x} = \frac{\partial [Hb]}{\partial x} = 0 \quad @ \; x = +0.5$$

which state that under the influence of the driving concentration gradient ($C_0 - C_1$), the hemoglobin-containing species are trapped in the membrane. The most useful result of the analysis is the flux of the permeant, $-D_A/L \partial [O_2]/\partial x$, at the membrane exit.

Much of the literature on facilitated transport is concerned with the steady-state solution applied to the following idealized second-order chemical reaction:

$$O_2 + Hb \leftrightarrow HbO_2 \qquad (4)$$

This reaction will be compared with the reaction

$$nO_2 + Hb \leftrightarrow HbO_{2n} \qquad (5)$$

which reproduces the experimental dissociation curve more accurately when n = 2.8 as shown as curve 2 in figure 1. It should be noted that the factor n is just an artifact used to match experimental data and is not an actual stoichiometric coefficient.

The kinetic constants k_1 and k_2 governing the rate of reaction are

$$R = k_1[O_2]^n[Hb] - k_2[HbO_{2n}] \qquad (6)$$

and the value of n is taken as either 1 or 2.8. The rate of reaction is a nonlinear function of the species concentration, and this is the main source of difficulty in solving the system of equations analytically.

With the assumption that the diffusivities of the hemoglobin-containing species are equal, which is quite good for this system, the relation between the Hb-containing molecules is simply (Kutchai et al., 1970)

$$[Hb] + [HbO_{2n}] = Q^* \qquad (7)$$

where Q^* is the total hemoglobin concentration (a constant in moles/cc).

Aside from the nonlinearity, the other major difficulty is the disparate time scale in equation 3 between the diffusive process (the space derivative term) and the chemical reaction (the forcing function). This important effect can best be illustrated with the aid of a linear model and an appropriate scaling. A common assumption used in the literature to linearize the facilitated transport problem (Noble et al., 1986) is that [Hb] is always at a constant level in equilibrium with $[O_2]$ and $[HbO_2]$. In the case of n=1:

$$[Hb] = \frac{k_2[HbO_2]}{k_1[O_2]} \qquad (8)$$

Eliminating the hemoglobin-oxygen complex from equations 7 and 8 yields the final formula for [Hb]:

$$[Hb] = \frac{Q^*}{1 + K[O_2]} \qquad (9)$$

where K is the equilibrium constant k_1/k_2. The oxygen concentration is some representative value such as the mean boundary concentration A_0. With one of the reacting species constant, the system of equations reduces to a coupled set of linear ordinary differential equations:

$$\begin{bmatrix} D_A & 0 \\ 0 & D_B \end{bmatrix} \begin{bmatrix} \dfrac{\partial^2 O_2}{\partial x^2} \\ \dfrac{\partial^2 [HbO_2]}{\partial x^2} \end{bmatrix} - \begin{bmatrix} \dfrac{k_1 Q^*}{1 + KA_0} & -k_2 \\ \dfrac{-k_1 Q^*}{1 + kA_0} & k_2 \end{bmatrix} \begin{bmatrix} [O_2] \\ [HbO_2] \end{bmatrix} = \begin{bmatrix} 0 \\ 0 \end{bmatrix} \tag{10}$$

For further analysis, it is useful to consider the system as a set of first-order ordinary differential equations. Let the vector $\underline{w}$ be defined as the nondimensional quantities $\{[O_2]/Q^*, [O_2]'/Q^*, [HbO_2]/Q^*, [HbO_2]'/Q^*\}^T$. The final 4×4 system of linear equations with constant coefficients is:

$$\begin{bmatrix} w_1' \\ w_2' \\ w_3' \\ w_4' \end{bmatrix} = \begin{bmatrix} 0 & 1 & 0 & 0 \\ \beta\dfrac{T_1}{T_3} & 0 & \dfrac{T_1}{T_4} & 0 \\ 0 & 0 & 0 & 1 \\ \beta\dfrac{T_2}{T_3} & 0 & \dfrac{T_2}{T_4} & 0 \end{bmatrix} \begin{bmatrix} w_1 \\ w_2 \\ w_3 \\ w_4 \end{bmatrix} \tag{11}$$

where primes denote x derivatives; the four relevant constants are

$$T_1 = L^2/D_A, \quad T_2 = L^2/D_B, \quad T_3 = 1/(k_1 Q^*), \quad T_4 = 1/k_2$$

and the factor β resulting from the linearization is $1/(1 + KA_0)$.

The constants T_1 through T_4 have the dimension of time, which, even though the problem is steady-state, have physical significance since the computed quantities represent transport rates. Unlike the transient problem considered in the following section, these parameters always appear as nondimensional ratios.

The first two scales relate to the diffusion of the permeant and carrier species, and the latter two relate to the forward and backward kinetic constants. The parameters D_A, D_B, k_1, and k_2 are fixed values for the O_2-Hb reaction while the membrane length L and the total Hb concentration Q^* are subject to variation in particular experiments. The second through fourth columns of table 1 show expected values of the constants for a representative range of the parameter L using the system parameters from Kutchai et al. (1970).

Since the forward chemical time constant T3 is so fast, the chemical reaction in equation 4 is heavily weighed toward the right. In addition, the diffusive time constants are quite large for increasing membrane thicknesses. Since the reciprocals of these diffusive time constants multiply the space derivatives, this term in equation 3 is generally small, which indicates chemical equilibrium. The dual constraint of satisfying the equation as well as the boundary conditions causes large deviations from equilibrium at the boundaries when the ratio of time constants is large. The details of the solution depend on all four time constants, out of which only three independent nondimensional parameters can be formed. The Damkohler number, defined as the ratio of the diffusive to chemical time scales, has often been used as a representative parameter. The system corresponding to L = 100 μ is characterized as one with a large Damkohler number and is referred to as a "fast" reaction. Such linear systems have been thoroughly examined in the literature by assuming equilibrium throughout, or by using the methods of asymptotic analysis.

The general solution of equation 11 is a sum of four exponentials that determine the spatial distribution, each having its own eigenvalue and eigenvector. The particular eigenvalues actually excited depends on the boundary conditions. Equation 11 has the property that the coefficient matrix possesses an eigenvalue equal to zero of rank 2. This simply means that equilibrium solutions (no chemical reaction) are admitted with a linear spatial gradient in [O_2]. A single parameter that characterizes the system is the absolute value of the remaining two eigenvalues which can be calculated from the coefficient matrix as

$$\lambda = \pm\sqrt{\beta \frac{T_1}{T_3} + \frac{T_2}{T_4}} \qquad (12)$$

The magnitude of the eigenvalue is computed for a range of membrane thicknesses and is also shown in table 1 along with the inverse of the eigenvalue which is a measure of the boundary layer thickness. Since one set of eigenvalues is always zero and the other set grows to very large values, this system of fast reactions is characterized as a stiff system. There is a large and growing literature concerning stiff systems of ordinary differential equations, mostly associated with initial value problems (Seider et al., 1982). In the case of facilitated transport, the stiffness becomes a problem associated with the boundary conditions as well as with the equations themselves, and is manifested by rapid spatial gradients near the boundaries.

SOLUTION OF THE FULL NONLINEAR EQUATIONS

The nonlinear time-dependent equations are solved by the method of time linearization using an implicit numerical algorithm with direct block tridiagonal solvers. In many applications it has been found to be advantageous to use direct solvers rather than iterative techniques whenever possible. In the unsteady implementation by Ruckenstein, an implicit algorithm was found to be more successful than earlier attempts using explicit methods. However, iterative techniques are needed to solve the resulting finite difference equations at each time step. Results are presented here using direct solvers for a range of cases from slow to very fast chemical reactions, including the temporal evolution of the transport process.

7

Most of the developments reported here on the use of implicit numerical methods for stiff systems of equations are based on work performed at NASA Ames Research Center in the 1960s on nonequilibrium aerodynamics. In Lomax and Bailey (1967) there is a complete discussion of the role of eigenvalues in choosing an appropriate numerical scheme for high-speed compressible flow. (It is interesting that the local linearization techniques presented in Gonzalez-Fernandez (1981) and Moretti (1965) are very similar, but are applied in two very different disciplines: biophysics and hypersonic gas dynamics, respectively.)

The method of time linearization involves the simple expedient of expanding the nonlinear term in a Taylor series about the solution at a previous time step. The first step is to discretize equation 3 in time using Euler forward differences:

$$\frac{\partial [O_2]}{\partial t} = \frac{[O_2] - [O_2]_p}{\Delta t}$$

$$\frac{\partial [HbO_2]}{\partial t} = \frac{[HbO_2] - [HbO_2]_p}{\Delta t}$$

(13)

where the subscript p refers to the previous value of the indicated quantity. Next, assemble the resulting equation in terms of the vector $\underline{w}$ defined previously

$$\underline{w}' = F(\underline{w}, \underline{w}_p)$$

where F is generally a nonlinear function of $\underline{w}$ at the current and previous time step. The linearized form is easily found by expanding F in a first-order vector Taylor series about $(\underline{w} - \underline{w}_p)$:

$$\underline{w}' = \underline{F}(w_p, w_p) + (\underline{w} - \underline{w}_p) \cdot \nabla \underline{F}(w_p, w_p)$$

The net result of this operation is to add two extra terms to the second and fourth rows of the coefficient matrix. It also affects the structure of the system by causing the coefficient matrix to vary in both space and time. Since no analytical solution is readily available for this linear problem, a numerical approach is necessary. In the development of such techniques for multidimensional problems with disparate scales, special methods, usually based on stretched coordinates, were developed. These "grid generators" are used to cluster the mesh in regions of high parameter variations. A typical application of this approach is discussed in Dwyer et al. (1982). In the current problem, with only one space dimension, it is useful to consider uniform grids to clearly highlight the resolution required to resolve the boundary effects. It is fortunate that the limit solution, that of complete chemical equilibrium, is a known boundary point for an infinitely dense grid.

The final system of equations is:

$$\underline{w}' = A\underline{w} + B$$

8

where A is the 4×4 coefficient matrix and B is a 4×1 vector. Both A and B depend upon $\underline{w}_p$. The matrix A is:

$$\begin{bmatrix} 0 & 1 & 0 & 0 \\[2ex] nw_{1_p}^{n-1}(1-w_{3_p})\dfrac{T_1}{T_3}+\dfrac{T_1}{\Delta t} & 0 & -w_{1_p}^n\dfrac{T_1}{T_3}-\dfrac{T_1}{T_4} & 0 \\[2ex] 0 & 0 & 0 & 1 \\[2ex] -nw_{1_p}^{n-1}(1-w_{3_p})\dfrac{T_2}{T_3} & 0 & w_{1_p}^n\dfrac{T_2}{T_3}+\dfrac{T_2}{T_4}+\dfrac{T_2}{\Delta t} & 0 \end{bmatrix}$$

The inhomogeneous right-hand side B is:

$$\begin{bmatrix} 0 \\[2ex] (1-n)w_{1_p}^n\dfrac{T_1}{T_3}+nw_{1_p}^n w_{3_p}\dfrac{T_1}{T_3}-w_{1_p}\dfrac{T_1}{\Delta t} \\[2ex] 0 \\[2ex] -(1-n)w_{1_p}^n\dfrac{T_2}{T_3}-nw_{1_p}^n w_{3_p}\dfrac{T_2}{T_3}-w_{3_p}\dfrac{T_2}{\Delta t} \end{bmatrix}$$

The system is solved with second-order central finite differences in vector form. Second-order forward and backward formulas are used at the boundaries to avoid including external mesh points.

After discretization, and incorporation of the boundary conditions, the solution vector $\underline{w}$ is easily computed using the block tridiagonal inversion algorithm described in Isaacson and Keller (1966). As mentioned above, one advantage of the matrix formulation is that more reactions and/or species can be accommodated by simply increasing the size of the blocks in the tridiagonal system.

CALCULATED SOLUTIONS

Membrane thickness is a dominant parameter in facilitated transport. Extremely thick or thin membranes can be analyzed using equilibrium or linearized methods, respectively. However, many problems of practical importance lie in the intermediate range.

Calculations are shown in figures 2 through 4 for membranes of thickness 1, 10, and 150 microns using the system parameters in table 1. Curves are shown for $X = [O_2]/C_0$ and $Y = [HbO_2]/Q^*$ from both linear and steady-state nonlinear calculations. Also shown are curves of oxyhemoglobin concentration

using local equilibrium values of X. At L = 1 µ the distribution of the oxygen permeant is predicted quite well using both linear and nonlinear theory. The deviation from complete equilibrium (a linear function of X vs. x), is slight, but more apparent is the discrepancy between the equilibrium curve and the two computed oxyhemoblobin distributions. There is a significant difference between the linear and nonlinear oxyheme distributions near the high pressure side of the membrane. The linear system in equation 11 is constrained to be symmetrical about x = 0, the midpoint of the membrane, which may account for the difference. The discrepancy between the nonlinear Y-curve and the equilibrium curve reverses sign at about x = 0.16. This indicates a reaction reversal in equation 6 and subsequent unloading of oxygen at the membrane exit.

Figure 3 shows the same dependent variables, but for a 10-micron-thick membrane. Here the discrepancy in the computed Y-distributions is obvious and the symmetry constraint seems to drive the oxyheme curve to values greater than one—a physically unrealistic result. Another tendency is for the oxygen concentration curves (X) to become more distorted, but with the side effect that chemical equilibrium is almost complete except for the strong deoxygenation of hemoglobin at the exit.

Figure 4 shows the most extreme case of L = 150 µ. Here the linear solution is obviously inapplicable and is not shown. The distribution of oxygen permeant is slightly more distorted, but the most important aspect of this curve is not at all obvious. This is the flux continuity constraint that forces the slope of the oxygen curve to match at entrance and exit, since this species is conserved within the membrane. The slope (or flux) changes very rapidly within the last one percent of the membrane. The governing equations can be manipulated in such a way (Fatt and La Force, 1965) that the flux can be accurately computed from the difference in oxyheme concentration across the membrane. The sensitivity of the flux (e.g., the difference in Y-values at entrance and exit) to the grid is shown in a sequence of five curves with 32, 64, 128, 256, and 512 mesh points. The grid size is shown to have an important effect on the computed flux. Figure 5 shows an expanded view of this region and shows clearly how the zero-slope boundary condition competes with the oxygen dissociation curve in such a way to induce rapid changes near the boundary. The extent of this region is directly related to the eigenvalues from the linear analysis as presented in equation 11.

The tendency toward equilibrium across the membrane is very strong. The only deviation is a very thin boundary-layer region where dissociation occurs in order to satisfy the boundary condition. Increasing mesh density shows an approach to an asymptotic value of Y which is just slightly above the equilibrium value. As mentioned above, the singular perturbation is such that the equilibrium value is always available as a lower limit. This effectively fixes the upper limit on the possible flux which can be computed using algebraic techniques. The size of this boundary-layer region can be approximated from the inverse eigenvalue (last column in table 1).

A calculation showing the unsteady evolution of the permeant is shown in figures 6 to 9 for the case L = 10 µ. All calculations are for a 512-point mesh interpolated to 50 points for clarity. Figure 6 depicts X as a function of space and time for two different initial concentrations—a linear and an exponential distribution. In both cases, chemical equilibrium was assumed in computing the initial values of Y. The linear initial distribution in figure 6(a) corresponds to the classical case of passive diffusion through a membrane with uniform flux throughout. The distribution of permeant adjusts very rapidly to the imbalance caused by the boundary condition constraint. This adjustment time is of the order of 0.3 sec which corresponds to the slow chemical time scale in table 1. The exponential distribution shown in figure 6(b)

is probably a more realistic initial condition since the starting flux vanishes at the membrane exit. Relaxation to steady state takes a little longer. Summary curves of entrance and exit flux are shown in figure 7 which give a better indication of the approach to steady state.

These results show that the steady-state solution is independent of initial conditions—an important physical confirmation of the mathematical model, since it is by no means assured that long-time solutions of nonlinear problems are independent of initial conditions.

Figures 8(a) and 8(b) are the direct counterparts of figure 6 except for the use of "sigmoid" shaped dissociation curves (specifically, curve 2 in figure 1). Aside from a different distribution of species in the steady state, the calculated data show a larger transient after the initial start. This transient seems to be concentrated in the low-pressure knee of the dissociation curve. The steady distribution of oxygen and oxyhemoglobin is shown in figure 9. A comparison with figure 3 shows the following dissociation curve effects: 1) Since the sigmoid curve has a high affinity for oxygen, there is very little free hemoglobin at the high-pressure boundary; 2) The boundary layer region near the low-pressure end of the membrane is wider. This indicates a reduction in stiffness in the governing equations with a less severe requirement on the number of grid points. Finally, figure 10 shows the approach to steady state as measured by the evolution of the entrance and exit flux. Note the slightly longer settling time and the enhanced excursion of the transient when compared with figure 7.

The most important single parameter in facilitated transport is the overall facilitation factor. Computed facilitation factors are compared with the experiments of Scholander and the computations of Kutchai in figure 11. As mentioned above, the facilitation factor is defined as the ratio of the oxygen flux through the membrane to the flux that would exist without a carrier species (Hb in this case) present. The definition used here is one greater than that used by Kutchai et al. (1970). The patterned line in figure 11 represents the experimental variation of F with variable pO_2. The crosses and open circles represent computations from Kutchai and the present code, respectively, using the hyperbolic dissociation curve. The slight differences are believed to be caused by the differing solubilities used in the two calculations. The solid circles represent results using the sigmoidal dissociation curve. Referring to figure 1, this curve is a better fit to the dissociation data, as reflected in the better agreement between theory and experiment.

This particular case is a good example of a stiff problem where the facilitation factor is quite close to the equilibrium value. This behavior is illustrated in figure 12 for the particular case $pO_2 = 25$ torr. Referring to figure 1, the operating region for the dissociation curve is the range $0 \leq pO_2 \leq 25$. The solid curve (dissociation curve 2) shows a more gradual fall in the normalized oxygen concentration at the low-pressure boundary when compared to the dashed curve (dissociation curve 1). Figure 13 shows a similar comparison for the oxyhemoglobin curves. As expected, the curve obtained using Hill's exponent is almost completely saturated at the high-pressure end of the membrane. Finally, figure 14 depicts the ratio of the flux of free oxygen to the total (free and oxygenated) flux across the membrane. A value of one indicates pure oxygen transport and a value of zero indicates oxyhemoglobin transport only. These curves indicate that the physically significant Hill's curve has a less-severe boundary layer effect and that only a small percentage of the oxygen is transported as a free species across the bulk of the membrane. This curve also clearly shows the region of active chemical reactions, as indicated by severe gradients. The beneficial effect of facilitated transport can be attributed to the fact that a rapid forward chemical reaction converts the oxygen to a combined form which is transported across the membrane in

11

this form. At the low-pressure end, the oxygen molecules are "dumped" in a reverse reaction. The strong asymmetry caused by the nonlinear interaction seems to be an important aspect of the transport process for this stiff problem.

CONCLUSIONS

A numerical study of unsteady facilitated transport of oxygen in the nonequilibrium range has been extended to model more realistic dissociation processes. A new analysis using implicit numerical schemes with direct tridiagonal solvers has been used to solve the governing reaction-diffusion equations.

The most important results from this analysis are: (1) Higher-order reaction models that better match oxygen dissociation curve data yield better agreement among theory and experiment for in vitro studies; (2) The linearized approximation can give useful information concerning the effect of the system parameters, but certain inherent symmetries of the linear theory cause serious errors in the facilitation factor as the equations become stiff; (3) The steady-state oxygen flux through a membrane is independent of the initial conditions; (4) The sigmoid oxygen dissociation curve causes almost 100% oxygen saturation in the high-pressure side of the membrane and increases the size of the boundary-layer region in the low-pressure side. This latter effect relaxes the stringent grid resolution problems using numerical methods.

The computational results reported in this paper were obtained on a VAX minicomputer. The analysis, however, is quite general and can be extended to greater space dimensions using more powerful computer resources to study more complex systems. It is expected that the unsteady aspects will be very important for biological systems since the characteristic diffusion time is probably larger than the molecular uptake time of a circulating red cell.

REFERENCES

Collins, R. E.: Transport of Bases through Hemoglobin Solution, Science, vol. 133, 19 May 1961, pp. 1593-1594.

Dwyer, H. A.; Smooke, M. D.; and Kee, R.: Adaptive Gridding for Finite Difference Solutions to Heat and Mass Transfer Problems, in Numerical Grid Generation, J. F. Thompson, ed., Elsevier Publ. Co., 1982.

Fatt, I.; and La Force, P.: Theory of Oxygen Transport through Hemoglobin Systems: A Model for Facilitated Membranous Transport, Science, vol. 147, no. 20, 1985, pp. 874-876.

Friedlander, S. K.; and Keller, L. H.: Mass Transfer in Reacting Systems near Equilibrium, Chem. Eng. Sci., vol. 20, 1965, pp. 121-129.

Goddard, J. D.; Schultz, J. S.; and Bassett, R. J.: On Membrane Diffusion with Near-Equilibrium Reaction, Chem. Eng. Sci., vol. 25, 1970, pp. 665-683.

Gonzalez-Fernandez, J. M.; and Atta, S.: Facilitated Transport of Oxygen in the Presence of Membranes in the Diffusion Path, Biophys. J., vol. 38, 1982, pp. 133-141.

Gonzalez-Fernandez, J. M.; and Atta, S.: Transport of Oxygen in Solutions of Hemoglobin and Myoglobin, Math. Biosciences, vol. 54, 1986, pp. 265-290.

Hemmingsen, E.; and Scholander, P. F.: Specific Transport of Oxygen through Hemoglobin Solutions, Science, vol. 132, no. 11, 1960, pp. 1379-1391.

Isaacson, E.; and Keller, H. B.: Analysis of Numerical Methods, J. Wiley, New York, 1966, p. 58.

Jain, R.; and Schultz, J.: Numerical Technique for Solving Carrier-Mediated Transport Problems, J. Membrane Sci., vol. 11, 1982, pp. 79-106.

Kutchai, H.; Jacquez, J. A.; and Matner, F. J.: Nonequilibrium Facilitated Oxygen Transport in Hemoglobin Solution, Biophys. J., vol. 10, 1970, pp. 38-54.

Lomax, H.; and Bailey, H. E.: A Critical Analysis of Various Numerical Integration Methods for Computing the Flow of a Gas in Chemical Nonequilibrium, NASA TN D-4109, 1967.

Lonsdale, H.: Reverse Osmosis, in P. M. Bungay et al., eds., Synthetic Membranes, Engineering and Applications, D. Reidel Publishing Co., 1986, pp. 307-342.

Moretti, G.: A New Technique for the Numerical Analysis of Nonequilibrium Flows, AIAA J., vol. 3, 1965, pp. 223-229.

Noble, R.; Way, J.; and Powers, L.: Effect of External Mass-Transfer Resistance on Facilitated Transport, Ind. Eng. Chem. Fund., vol. 25, 1986, pp. 450-452.

Ruckenstein, E.; and Varanasi, S.: Transport Behavior of Facilitated Transport through Liquid Membranes, J. Membrane Sci., vol. 12, 1982, pp. 27-50.

Schultz, J.: Carrier Mediated Transport, in P. M. Bungay et al., eds., Synthetic Membranes, Engineering and Applications, D. Reidel Publishing Co., 1986, pp. 523-566.

Schultz, J. S.; Goddard, J. D.; and Suchdeo, S. R.: Facilitated Transport via Carrier-Mediated Diffusion in Membranes, AICHE J., vol. 20, 1974, pp. 417-445.

Scholander, P. F.: Oxygen Transport through Hemoglobin Solutions, Science, vol. 131, no. 26, 1960, pp. 585-590.

Seider, W. D.; White, C. W.; and Prokopakis, G. J.: Stiff Ordinary Differential Equations in Chemical Process Analysis, Proc. Intl. Conf. on Stiff Computation, Salt Lake City, Utah, 1982.

Stryer, L.: Biochemistry, W. H. Freeman Co., San Francisco, 1981.

Varanasi, S.; and Ruckenstein, E.: Relaxation Methods for Facilitated Transport, J. Membrane Sci., vol. 13, 1983, pp. 67-84.

Wang, J. H.: Transport of Oxygen through Hemoglobin Solutions, Science, vol. 133, no. 2, 1961, pp. 1770-1771.

TABLE 1– Expected Values of Time Constants for Facilitated Transport of Oxygen through Hemoglobin Solution

$D_A = 1.45 \times 10^{-5}$ cm^2/sec
$D_B = 3.00 \times 10^{-7}$ cm^2/sec
$k_1 = 3.18 \times 10^9$ (sec-moles/cc)$^{-1}$
$k_2 = 40$ sec^{-1}
$Q^* = 10 \times 10^{-6}$ moles/cc
$pO_2 = 100$ torr at entrance
$\alpha = 1.7 \times 10^{-9}$ moles/cc/torr
$C_0 = 1.7 \times 10^{-7}$ moles/cc
$C_1 = 0.0$

L	T_1, sec	T_2, sec	T_3, sec	T_4, sec	λ	$1/\lambda$
1	0.00069	0.0333	0.0000314	0.025	2.04	0.4902
10	0.0690	3.33	0.0000314	0.025	20.4	0.04902
100	6.90	333	0.0000314	0.025	204	0.00490
150	15.5	750	0.0000314	0.025	306	0.00327
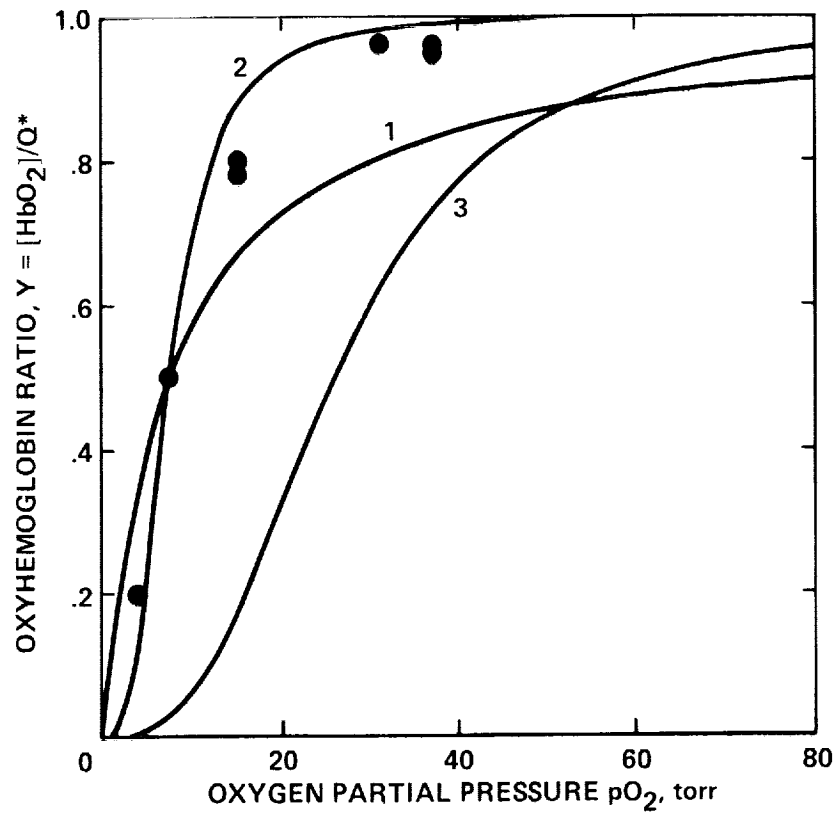
Figure 1.– Dissociation curves for oxygen transport through hemoglobin solution. Curve 1, Second-order chemical reaction, $pO_{2,0.5}$ = 7.4 torr; Curve 2, Sigmoid dissociation curve, $pO_{2,0.5}$ = 7.4 torr; Curve 3, Sigmoid dissociation curve for physiological conditions, $pO_{2,0.5}$ = 26 torr. Symbols, experiment (Hemmingsen, 1960).
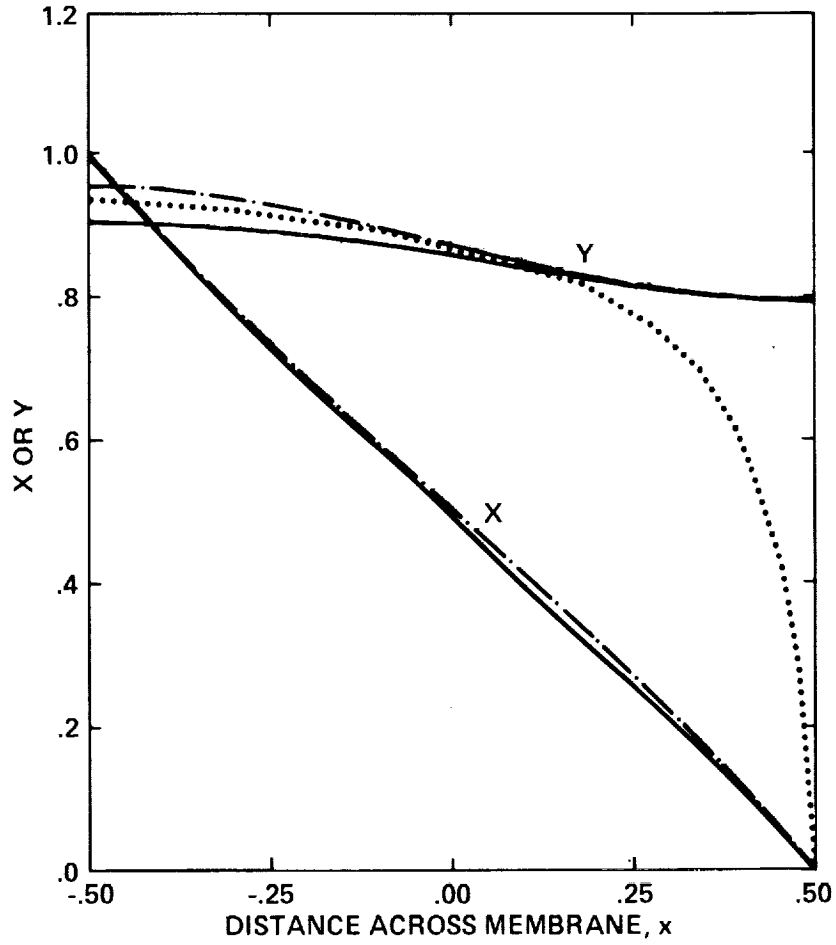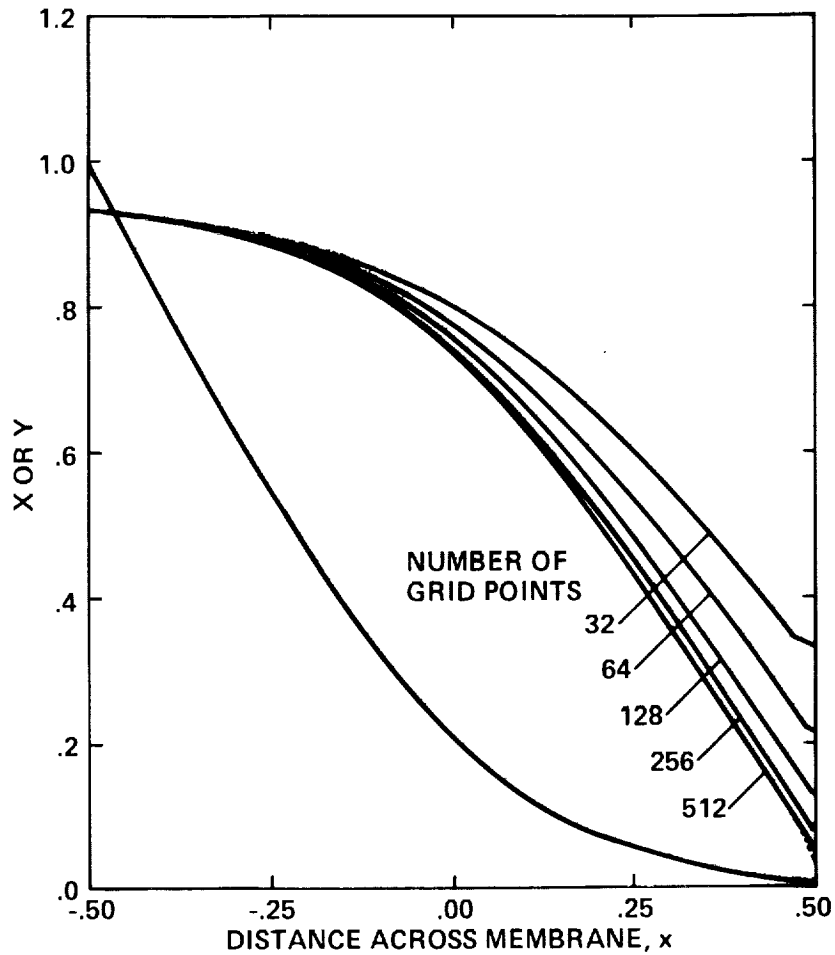
Figure 2.– Distribution of X = $[O_2]/C_0$ and Y = $[HbO_2]/Q^*$ across the membrane. Second-order chemical reaction, L = 1 micron, pO_2 = 100 torr at entrance, 0 at exit. _____, nonlinear calculation; — — — —, linear calculation; ...., equilibrium curve Y(X).

17
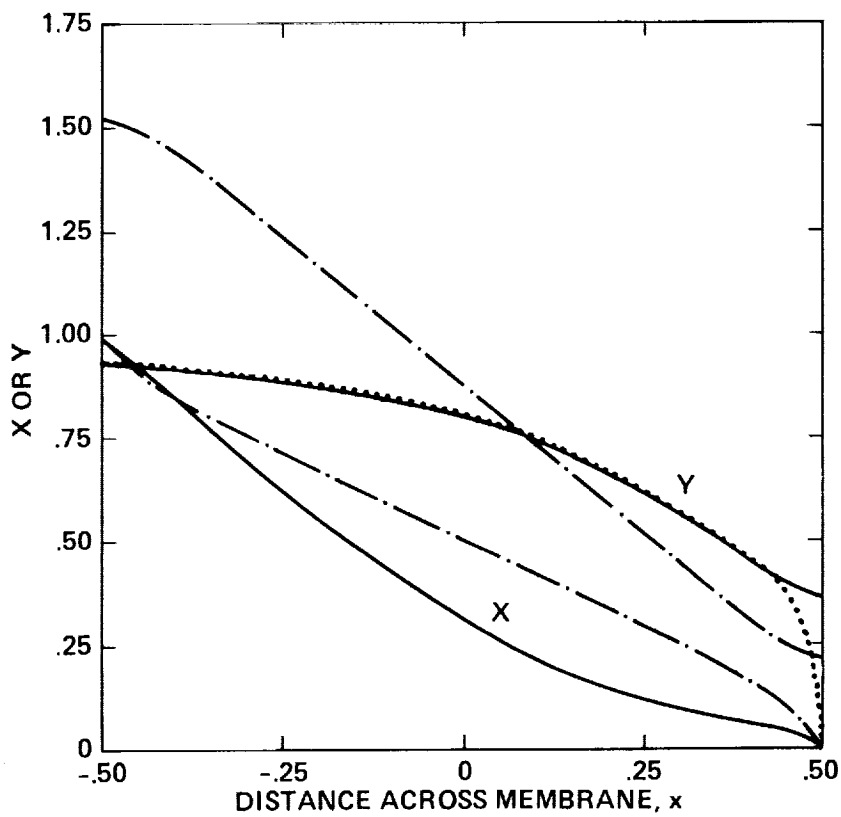
Figure 3.– Distribution of X = [O$_2$]/C$_0$ and Y = [HbO$_2$]/Q* across the membrane. Second-order chemical reaction, L = 10 microns, pO$_2$ = 100 torr at entrance, 0 at exit. _____, nonlinear calculation; — — —, linear calculation; ...., equilibrium curve Y(X).

18

Figure 4.— Distribution of X = $[O_2]/C_0$ and Y = $[HbO_2]/Q^*$ across the membrane. Second-order chemical reaction, L = 150 microns, pO_2 = 100 torr at entrance, 0 at exit. _____, nonlinear calculation; — — — — —, equilibrium curve Y(X). Curves of Y shown for 5 different computational grids.
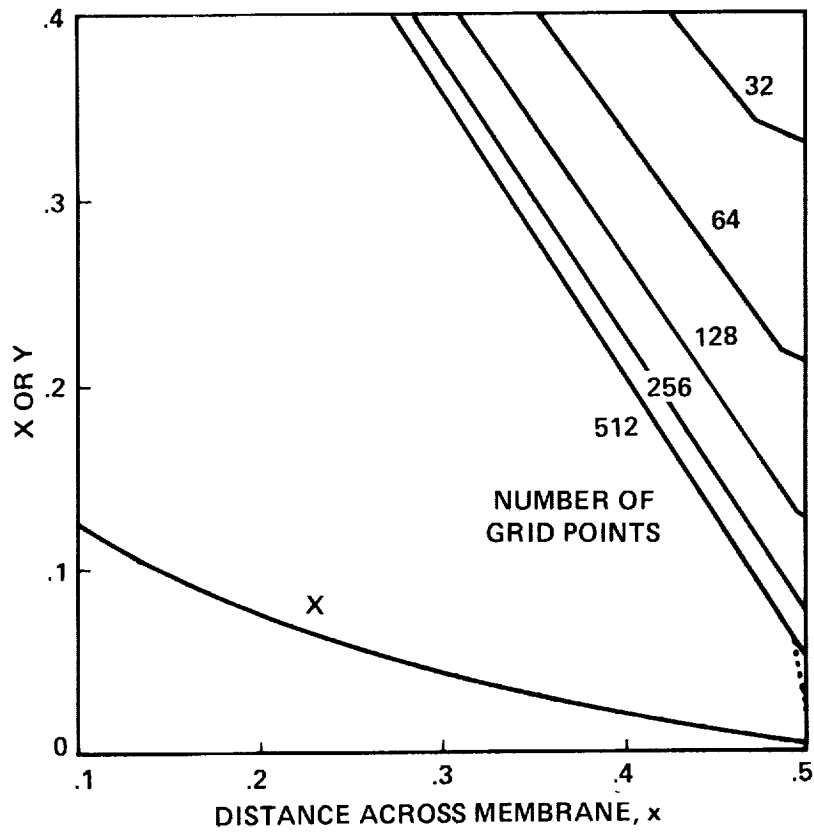
Figure 5.– Same conditions as figure 4 showing low-pressure side of membrane.
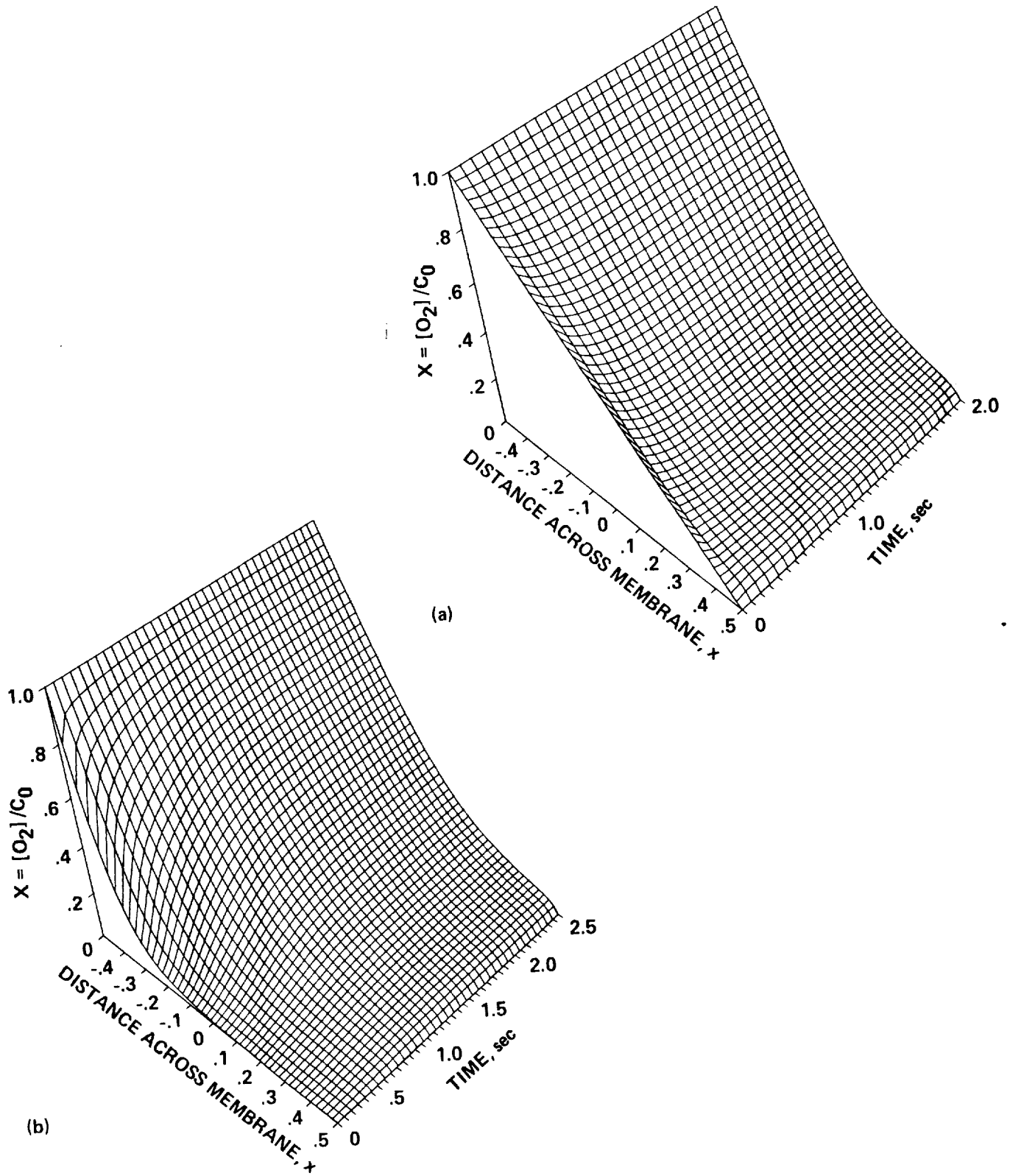
Figure 6.– Space-time distribution of oxygen concentration. Second-order chemical reaction,
L = 10 microns, pO₂ = 100 torr at entrance, 0 at exit. a) Constant flux (linear) initial distribution,
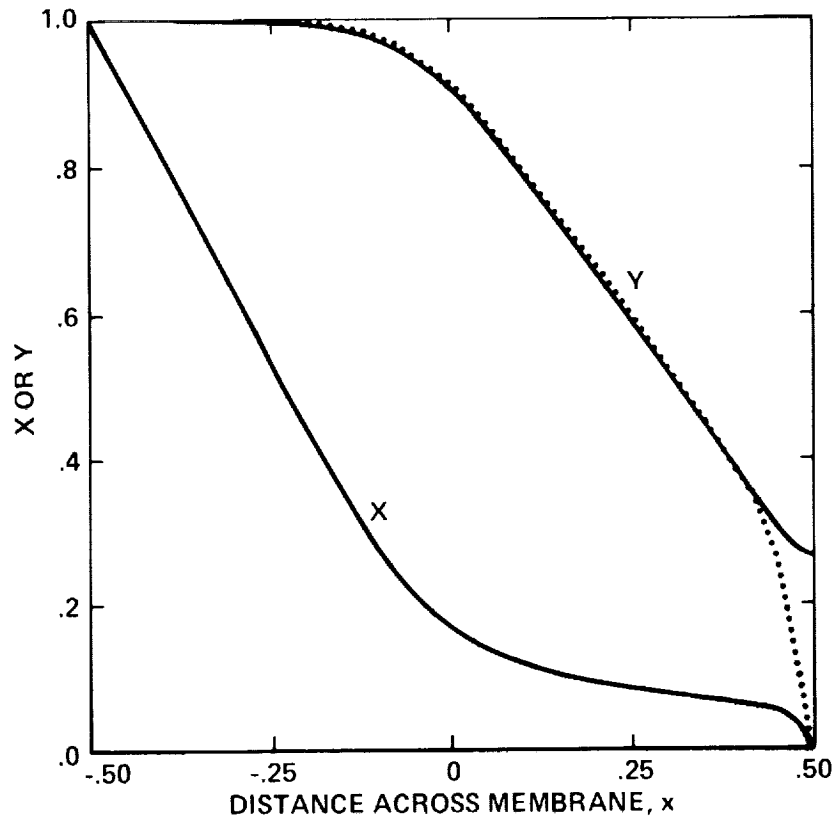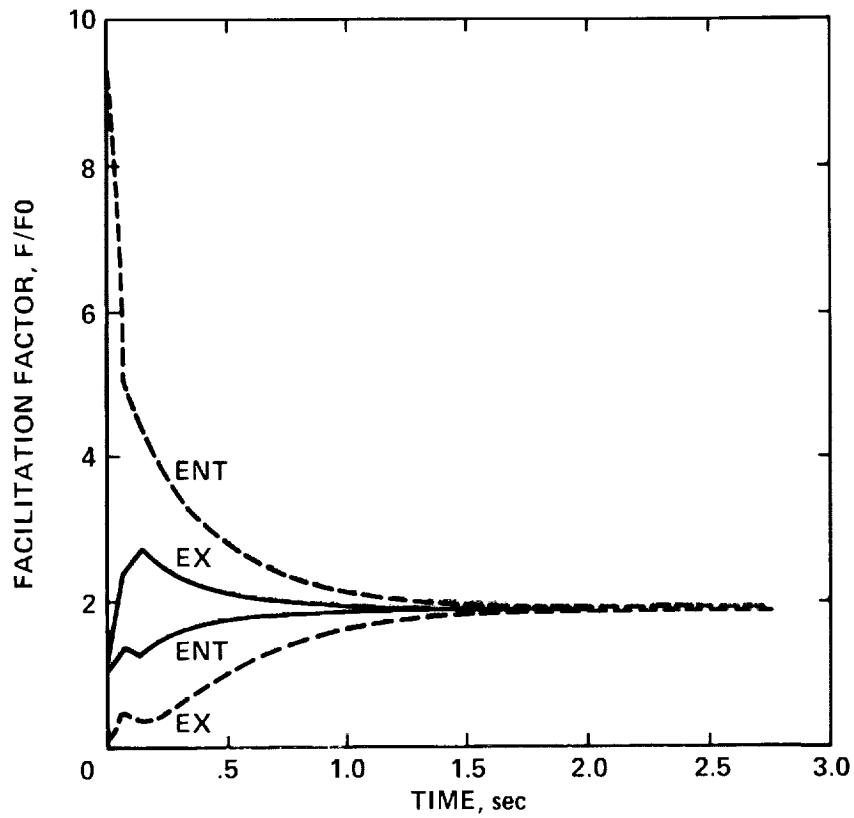b) variable flux (exponential) initial distribution.
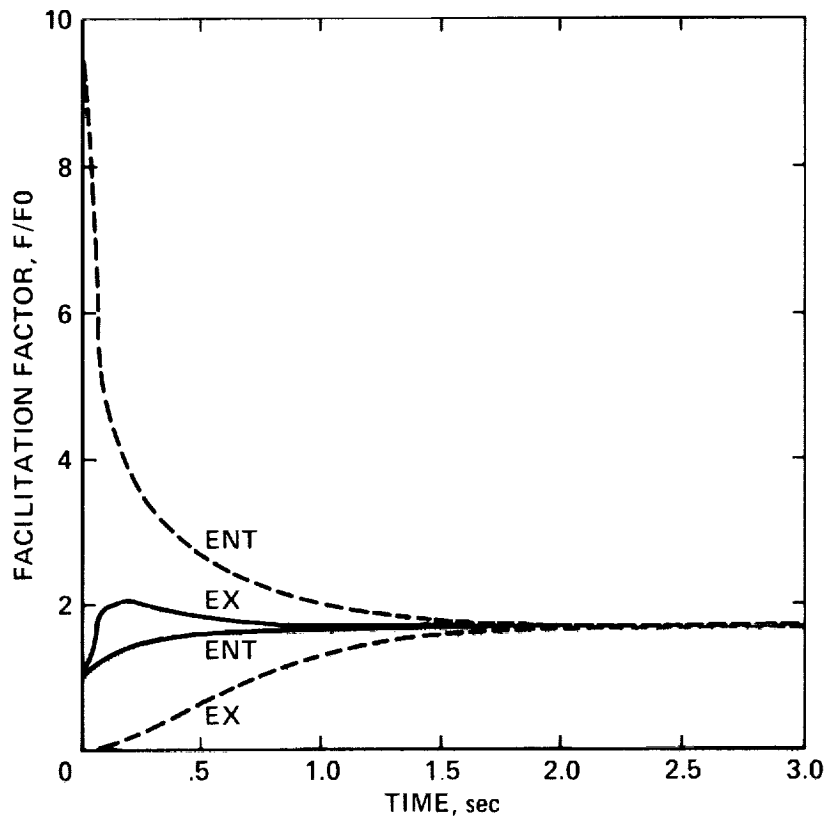
Figure 7.– Transient flux (normalized by flux without chemical reaction, F_0) at entrance (ENT) and exit (EX) of membrane. Same parameters as figure 6. _____, linear initial distribution; – – – – – –, exponential initial distribution.
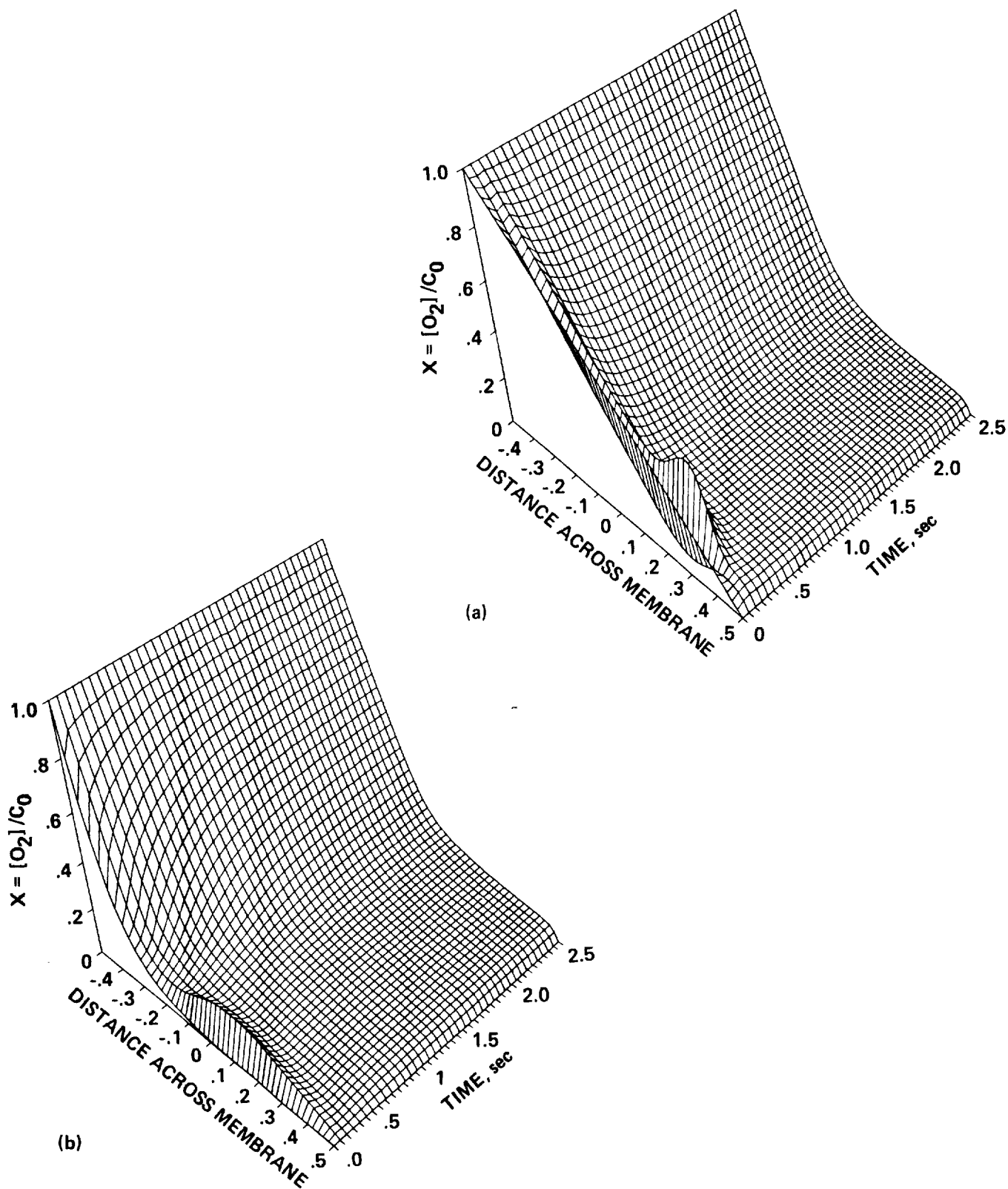
Figure 8.– Space-time distribution of oxygen concentration. Sigmoid dissociation curve, L = 10 microns, pO_2 = 100 torr at entrance, 0 at exit. a) Constant flux (linear) initial distribution, b) variable flux (exponential) initial distribution.

23

Figure 9.– Distribution of X = [O_2]/C_0 and Y = [HbO_2]/Q^* across the membrane. Sigmoid dissociation curve, L = 10 microns, pO_2 = 100 torr at entrance, 0 at exit. _____, nonlinear calculation; — — — —, linear calculation; ...., equilibrium curve Y(X).

Figure 10.– Transient flux (normalized by flux without chemical reaction, F_0) at entrance (ENT) and exit (EX) of membrane. Same parameters as figure 8. _____, linear initial distribution; – – – – –, exponential initial distribution.
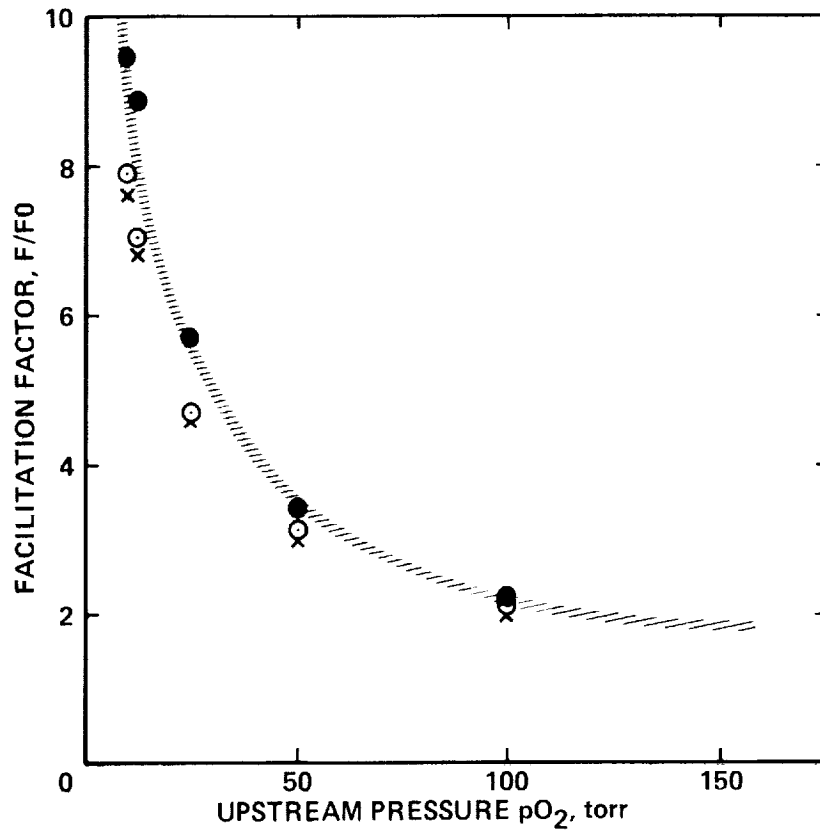
Figure 11.– Variation of steady-state facilitation factor with oxygen partial pressure at membrane
entrance. L = 150 microns, other parameters as in table 1. = = = = = =, experiment (Scholander);
solid symbols, sigmoid dissociation curve; open symbols, second-order dissociation curve; crosses,
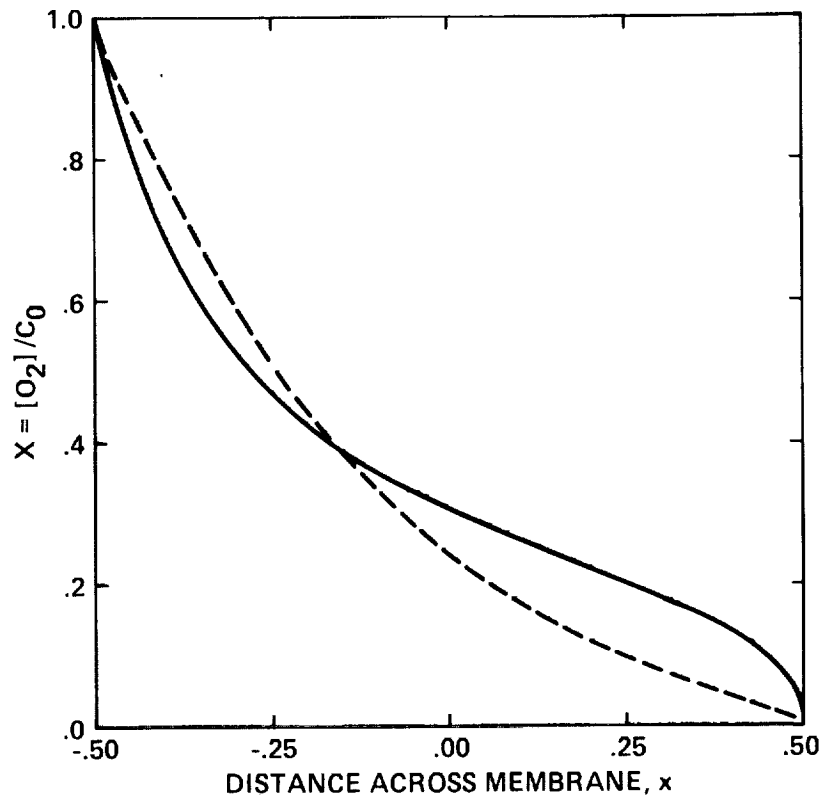computation (Kutchai) using second-order dissociation curve.

Figure 12.– Comparison of X = [O_2]/C_0 distributions across a membrane. pO_2 = 25 torr at entrance. _____, sigmoid dissociation curve; — — — — —, second-order dissociation curve.
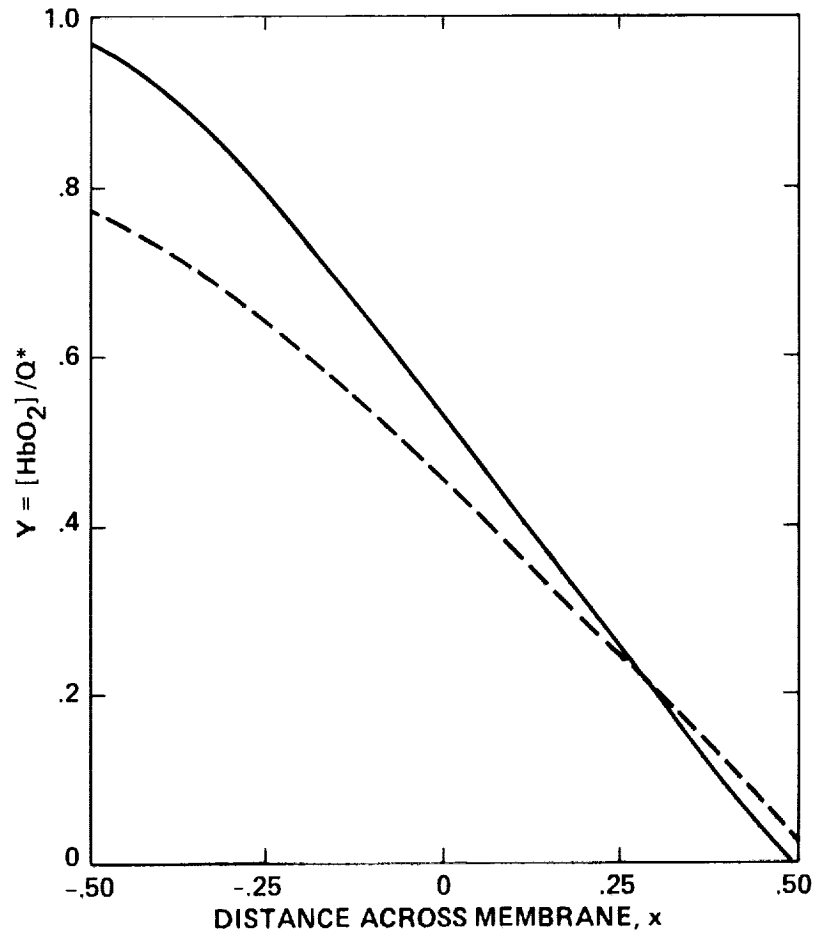
Figure 13.– Comparison of $Y = [HbO_2]/Q^*$ distributions across a membrane. $pO_2 = 25$ torr at entrance. _____, sigmoid dissociation curve; – – – – –, second-order dissociation curve.
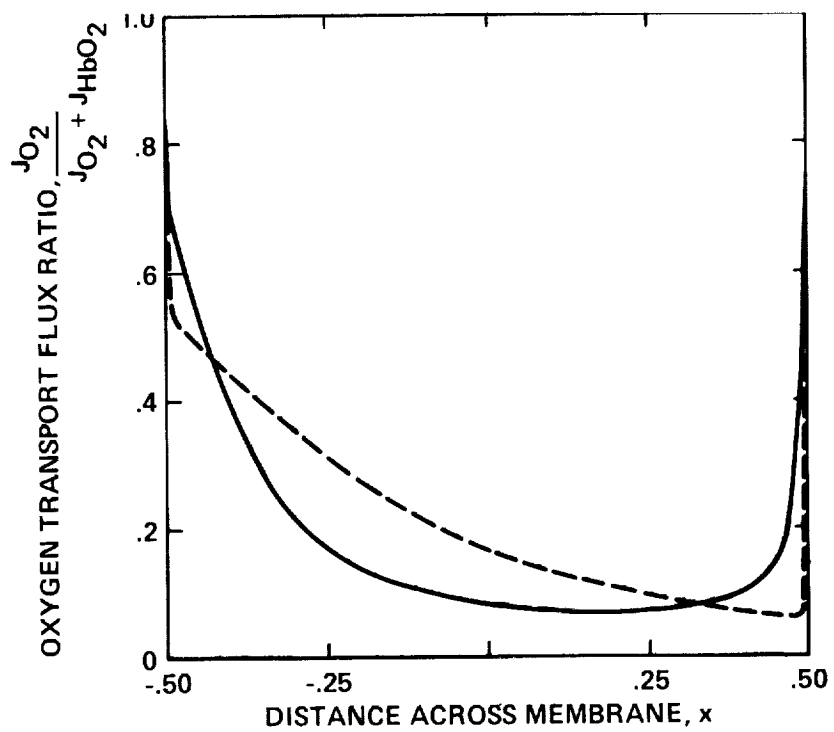
28

Figure 14.– Transport of free oxygen fraction across a membrane. $pO_2 = 25$ torr at entrance. _____,
sigmoid dissociation curve; — — — — —, second-order dissociation curve.

Report Documentation Page

1. Report No. NASA TM-102251	2. Government Accession No.	3. Recipient's Catalog No.

4. Title and Subtitle Computation of the Unsteady Facilitated Transport of Oxygen in Hemoglobin	5. Report Date January 1990
	6. Performing Organization Code

7. Author(s) Sanford Davis	8. Performing Organization Report No. A-90011
	10. Work Unit No. 505-61-31

9. Performing Organization Name and Address Ames Research Center Moffett Field, CA 94035-1000	11. Contract or Grant No.
	13. Type of Report and Period Covered Technical Memorandum

12. Sponsoring Agency Name and Address National Aeronautics and Space Administration Washington, DC 20546-0001	
	14. Sponsoring Agency Code

15. Supplementary Notes

Point of Contact: Sanford Davis, Ames Research Center, MS 260-1, Moffett Field, CA 94035-1000
(415) 604-4197 or FTS 464-4197

16. Abstract

The transport of a reacting permeant diffusing through a thin membrane is extended to more realistic dissociation models. A new nonlinear analysis of the reaction-diffusion equations, using implicit finite-difference methods and direct block solvers, is used to study the limits of linearized and equilibrium theories. Computed curves of molecular oxygen permeating through hemoglobin solution are used to illustrate higher-order reaction models, the effect of concentration boundary layers at the membrane interfaces, and the transient buildup of oxygen flux.

17. Key Words (Suggested by Author(s)) Facilitated transport Oxygen-hemoglobin system Membranes	18. Distribution Statement Unclassified-Unlimited Subject Category - 55

19. Security Classif. (of this report) Unclassified	20. Security Classif. (of this page) Unclassified	21. No. of Pages 32	22. Price A03